

Loss of single-walled carbon nanotubes selectivity by disruption of the Co–Mo interaction in the catalyst

José E. Herrera and Daniel E. Resasco *

School of Chemical Engineering and Materials Science, University of Oklahoma, 100 East Boyd Street, Norman, OK 73019, USA

Received 24 June 2003; revised 8 August 2003; accepted 11 August 2003

Abstract

In previous work, we reported the growth of well-structured single-walled carbon nanotubes (SWNT) by CO disproportionation on Co:Mo/SiO₂ catalysts. We have proposed that high SWNT selectivity can only be obtained when most of the Co in the sample is interacting with Mo and forming a cobalt–molybdate surface layer. In this contribution, we report further evidence to the hypothesis by an investigation of Na-doped Co:Mo/SiO₂ catalysts. The effect of the sodium addition has been investigated by Raman spectroscopy, ultraviolet–visible diffuse reflectance spectroscopy, H₂ temperature-programmed reduction, and X-ray photoelectron spectroscopy. The results are compared to those obtained in a previous study on undoped CoMo/SiO₂ catalysts. Significant differences are observed between the undoped and Na-doped catalytic systems. It has been found that the presence of sodium favors the dispersion of molybdenum, which tends to form sodium molybdate species over the silica support. At the same time, the formation of these sodium molybdate structures hinders the interaction between cobalt and molybdenum, preventing the formation of the cobalt molybdate species. This disruption has been found to be detrimental to the SWNT selectivity of the catalyst, giving further evidence to the link between the presence of this surface species and the selective SWNT growth.

© 2003 Elsevier Inc. All rights reserved.

Keywords: Single-walled carbon nanotubes; Raman; XPS; TPR; UV–vis/DRS; TPO; Co Mo catalyst; Na

1. Introduction

Single-wall carbon nanotubes (SWNT) can be considered as one of the building blocks for nanoscale science and nanotechnology. They exhibit exceptional chemical and physical properties that have opened a vast number of potential applications [1]. Extensive research work is now focused on the large-scale manufacture of these materials at low cost since there is not yet an established method that provides large quantities of SWNT of well-determined and reproducible characteristics. A clear understanding of the formation mechanism of SWNT is therefore a key issue for the development of further advances in this topic.

Several SWNT growth mechanisms have been proposed [2–5]; most of them involve the interaction of carbon species with a metal (atom, cluster, solution, carbide, etc.), which in turn depends on the method used to synthesize the SWNT. Our group has focused on the disproportionation of CO on bimetallic catalysts. We have previously reported

that among the various formulations investigated, Co–Mo catalysts supported on silica gel and having low Co:Mo ratios exhibited the best performance [6,7]. We have explained this performance on the basis of a Co–Mo interaction that is critical for the performance of the catalyst [8]. Separated, these metals are not effective; they are either inactive (Mo alone) or unselective (Co alone). The catalyst is only effective when both metals are simultaneously present with a low Co:Mo ratio. Through a detailed characterization that involved a variety of characterization techniques such as EXAFS, XANES, UV–vis/DRS, XPS, and DRIFTS of adsorbed NO, we were able to explain the reasons for the high selectivity of these catalysts [8].

Interestingly, the Co–Mo system is a catalyst commonly employed in petroleum refining for hydrotreating processes. However, most studies on these catalysts have focused on alumina-supported systems since alumina interacts with the metals with the appropriate strength to generate the species with the optimum hydrotreating activity in the sulfided state. After many years of intense research by several groups the structure of the sulfide Co–Mo catalysts is now known at the atomic level [9–12]. Other characteristics of these cata-

* Corresponding author.

E-mail address: resasco@ou.edu (D.E. Resasco).

lysts have also been investigated, such as the influence of alkali dopants on their structure and activity [13–16]. There is still some controversy about this issue in the literature, although it seems clear that the presence of these dopants predominantly affects the dispersion of molybdenum species [16–20].

In the present contribution, we have turned our attention to study the effect of the presence of sodium in the Co–Mo catalytic system for the SWNT production. As noted above, in our proposed model, the interaction of Co and Mo is critical for a good catalyst performance. Therefore, the introduction of an element such as sodium that will compete with Co for the interaction with molybdenum is expected to be detrimental for the catalytic selectivity. We have followed a characterization strategy on the basis of the abundant precedent literature and our own work to investigate this multicomponent system. Based on the results of this characterization, we have put together a schematic picture of the doped catalyst, and built up an analogy with the undoped Co–Mo system, which can be used to explain the variations in selectivity toward SWNT observed when the catalyst is doped with sodium.

2. Experimental

2.1. Catalysts preparation and pretreatment

A series of Na-doped and undoped silica-supported Co–Mo catalysts was prepared. For the Na-doped catalysts different amounts of sodium were added to the SiO₂ support by incipient wetness impregnation using aqueous solutions of NaNO₃ of appropriate concentrations. The SiO₂ support obtained from Aldrich had an average pore size of 6 nm, BET area 480 m²/g, pore volume 0.75 cm³/g, and particle sizes in the range 70–230 mesh. After evaporation of water at room temperature, the solid was dried at 110 °C overnight and then calcined at 500 °C for 3 h. Subsequently, the Na-doped and undoped supports were loaded with molybdenum (4.6 wt%) and cobalt (1.4 wt%) by incipient wetness coimpregnation of a solution of cobalt nitrate and ammonium heptamolybdate to achieve a Co:Mo molar ratio of 1:3. After impregnation, the solids were dried overnight at 120 °C and then calcined for 3 h at 500 °C in dry-air flow. Two monometallic Na-doped catalysts were also prepared, containing 1.3 wt% Co and 4.6 wt% Mo.

2.2. Catalyst characterization

The Raman spectra of calcined catalysts were obtained in a Jovin Yvon-Horiba LabRam 800 equipped with an air-cooled CCD detector equipped with a He–Ne laser (632.8 nm). Typical laser powers ranged from 1.0 to 2.0 mW; integration times were around 15 s for each spectrum; 10 Raman spectra were averaged for each sample.

The UV–vis spectra of the calcined catalysts were recorded using a Shimadzu double beam spectrometer UV-2101 with an integrating sphere for diffuse reflectance. Barium sulfate was used as reflectance standard. Several Mo and Co compounds, including MoO₃, Na₂MoO₄, (NH₄)₆Mo₇O₂₄, and CoMoO₄ were used as references. Before analysis, the samples were dried in air at 120 °C.

Temperature-programmed reduction (TPR) experiments were conducted passing a continuous flow of 5% H₂/Ar over approximately 30 mg of the calcined catalyst at a flow rate of 10 cm³/min, while linearly increasing the temperature at a constant heating rate of 8 °C/min. The hydrogen uptake as a function of temperature was monitored using a thermal conductivity detector, SRI Model 110 TCD.

X-ray photoelectron spectroscopy data were recorded on a Physical Electronics PHI 5800 ESCA System with monochromatic Al-K_α X-rays (1486.6 eV) operated at 350 W and 15 kV with a background pressure of approximately 2.0 × 10⁻⁹ Torr. A 400-μm spot size and 58.7-eV pass energy were typically used for the analysis. Sample charging during the measurements was compensated by an electron flood gun. The electron takeoff angle was 45° with respect to the sample surface. For each sample, the binding energy regions corresponding to Si (95–115 eV), Mo (220–245 eV), and Co (760–820 eV) were scanned. The binding energies were corrected by reference to the C(1s) line at 284.8 eV. A nonlinear Shirley-type background was used for the area analysis of each peak. The fitting of the XPS spectra was carried out with Gaussian–Lorentzian peaks, using the MultiPak software from Physical Electronics.

2.3. Production and characterization of carbon nanotubes

For the SWNT production, 0.5 g of calcined catalyst was placed in a horizontal tubular reactor, heated in H₂ flow up to 500 °C, and then in He flow up to 850 °C. Subsequently, CO was introduced at a flow rate of 850 cm³/min at 80 psia and kept under these conditions for 2 h. At the end of each run, the system was cooled down in He flow. The total amount of carbon deposits was determined by temperature-programmed oxidation (TPO) following the method described in our previous work [6]. Since Na has an inherent catalytic effect on oxidation processes and might affect the position of the peaks, before each TPO analysis undoped catalyst samples were impregnated with a solution of sodium nitrate to get a total loading of 4% Na and heated in He to decompose the inorganic salt.

Transmission electron microscopy (TEM) was used to analyze the quality of the nanotubes obtained over the different catalysts. The TEM images were obtained in a JEOL JEM-2000FX TEM. For this analysis, a suspension of the carbon-containing samples was achieved by ultrasound stirring the solid sample in isopropanol for 10 min. A few drops of the resulting suspension were deposited on a grid and subsequently evacuated before the TEM analysis.

The quality of the nanotubes was also examined by Raman spectroscopy, one of the most powerful techniques available to study the structural and electronic properties of SWNT. The analysis of radial A_{1g} breathing mode (below 300 cm^{-1}) gives direct information about the tubes diameter [21], while the analysis of the G band in the tangential mode range, i.e., $1400\text{--}1700\text{ cm}^{-1}$, provides information on the electronic properties of the nanotubes. In addition, the analysis of the so-called D band at around 1350 cm^{-1} gives an indication of the level of disordered carbon. Therefore, we have used the intensity ratio of the D band (1350 cm^{-1}) to the G band (1590 cm^{-1}) as semiquantitative measurement of the formation of undesirable forms of carbon [22,23].

3. Results

3.1. Characterization of the catalysts

3.1.1. Raman spectroscopy

Raman spectroscopy has shown to be an extremely powerful tool for characterizing supported heterogeneous catalysts containing d^0 transition metal oxide species [17]. In fact, substantial information about the dispersion of molybdenum oxide species over the high surface-area support has been obtained from detailed analysis of Raman spectra [19, 24–28]. Those studies provide the basis for interpreting the results of the present catalyst characterization. Fig. 1 shows the Raman spectra of an undoped Co:Mo (1:3)/SiO₂ and of two Na-doped Co:Mo (1:3)/SiO₂ catalyst; the Raman spectra of reference samples of cobalt oxide (Co₃O₄), cobalt molybdate (CoMoO₄), and sodium molybdate (Na₂MoO₄) are also shown in the figure.

Fig. 1a compares the Raman spectrum of the undoped and Na-doped catalysts with that of a CoMoO₄ reference sample. The peaks appearing in the $750\text{--}1000\text{ cm}^{-1}$ region should be ascribed to Mo species. This is the region where the bands for stretching of Mo–O bonds are typically observed [17]. Several factors such as metal loading, pH, precursor, impregnation method, and impurities are known to influence the exact position of the Raman bands. However, a preliminary assignment can be done based on the preceding literature and the comparison with the reference samples. For instance, in the case of the undoped catalyst the peak centered at 943 cm^{-1} has been previously ascribed to Mo₇O₂₄^{−6} species while the shoulder at 960 cm^{-1} has been associated with larger clusters of MoO_x species, such as Mo₈O₂₆^{−4} [17,27,28]. This assignment is in good agreement with our previous UV–vis spectroscopy results [8], which suggested the presence of well-dispersed clusters of MoO_x. According to the calculated band energy gap, the average domain size of these species was estimated to be slightly larger than that of Mo₇O₂₄^{−6}. At the same time, the presence of large polymeric MoO_x species must be ruled out when there are no peaks in the $990\text{--}1000\text{ cm}^{-1}$ region [20,29], a conclusion that we also indicated based on the

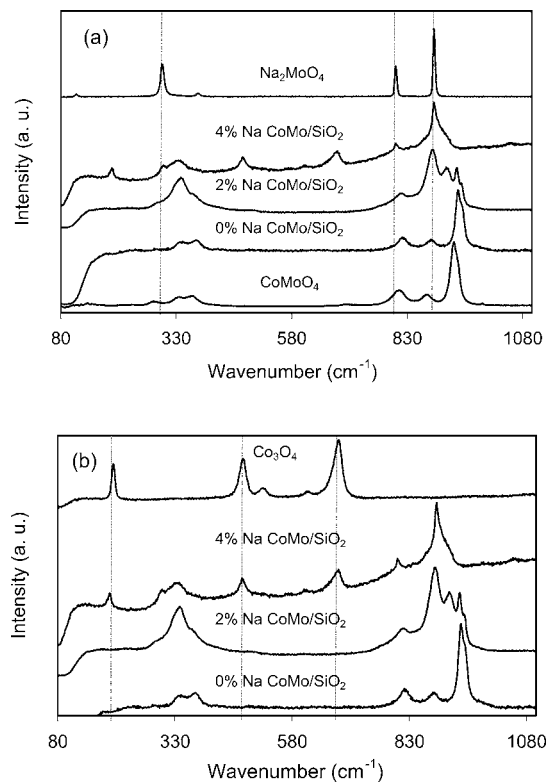


Fig. 1. Raman spectra of an undoped and two Na-doped Co:Mo (1:3)/SiO₂ catalysts compared to (a) the spectra of two analytical samples of cobalt molybdate (CoMoO₄) and sodium molybdate (Na₂MoO₄) and compared to (b) the spectrum obtained for a reference sample of cobalt oxide Co₃O₄. The laser excitation energy was 633 nm.

previous UV–vis data [8]. Moreover, a comparison of the Raman spectrum of the undoped bimetallic catalyst with that of the CoMoO₄ gives strong support to the presence of this type of species. Therefore, the Raman band at 880 cm^{-1} , the shoulder at 930 cm^{-1} , and the broad band at 350 cm^{-1} must all be assigned to Mo–O–Co stretching vibrations in cobalt molybdate-like species [27,30–33].

A noticeable change in the Raman bands is observed when sodium is present in the catalyst. First of all, when inspecting the spectrum of the for the Na-doped Co:Mo (1:3)/SiO₂ catalysts, a new band at 889 cm^{-1} becomes prominent. This band has been previously assigned to Mo=O stretching of isolated monooxo (MoO₄^{−2}) species [34]. Also, the band at 825 cm^{-1} (asymmetric Mo–O–Mo stretching) shows a dramatic shift to lower wavenumbers (805 cm^{-1}), which is consistent with a decrease in the amount of Mo–O–Mo moieties on the catalysts when sodium is present in the sample. It is also important to note that the bands assigned to Co–O–Mo species present on the undoped catalyst ($350, 880, \text{ and } 930\text{ cm}^{-1}$) become very weak until they almost totally vanish for the catalyst with the higher Na loading.

Fig. 1b shows a comparison of the Raman spectra of the Na-doped catalysts with the spectrum of the cobalt oxide reference. The assignments for the Raman active phonon

modes that are displayed in the spectrum of Co_3O_4 are as follows. The peaks at 199, 621, and 681 cm^{-1} correspond to F_{2g} phonon modes, while the peaks at 477 and 525 cm^{-1} are E_g and A_{1g} phonon modes, respectively [35]. As seen in Fig. 1b, this set of peaks is undoubtedly present in the spectrum of the 4% Na-doped catalyst, while it is entirely absent in the case of the undoped catalyst. From this evidence, it is clear that segregated Co_3O_4 species are not present on the undoped catalyst while the addition of Na seems to favor the formation a new segregated cobalt oxide phase.

3.1.2. Diffuse reflectance UV–visible spectroscopy (UV–vis/DRS)

We have used UV–vis/DRS to study the state of both Mo and Co in the fresh catalyst. In order to estimate the band energy gap of d^0 oxides, it has been recommended to use the square root of the Kubelka–Munk function multiplied by the photon energy, and to plot this new function versus the photon energy [36]. The position of the absorption edge can then be determined by extrapolating the linear part of the rising curve to zero. The values thus obtained carry information about the average domain size of the oxide nanoparticles. It has been shown that the energy band gap decreases as the domain size increases [36,37]. Therefore, a comparison can be made between the energy of the samples under investigation and those of references of known domain size. This comparison is made in Fig. 2, which shows the absorption edges of several MoO_x species together with those of two different Na-doped and an undoped Co:Mo (1:3)/ SiO_2 catalysts. As expected, the band gap energies in the ref-

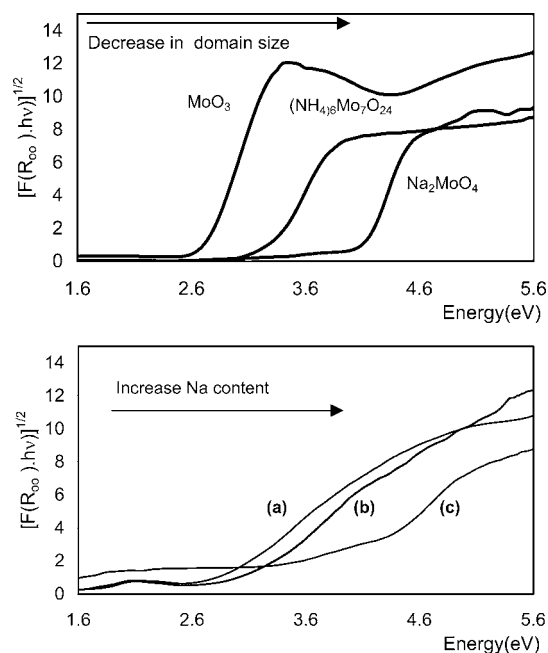


Fig. 2. Lower panel: UV absorption spectra for (a) an undoped Co:Mo (1:3)/ SiO_2 catalysts, (b) 2.0 wt% Na-doped Co:Mo (1:3)/ SiO_2 catalyst, and (c) a 4.0 wt% Na-doped Co:Mo (1:3)/ SiO_2 catalyst. Upper panel: UV absorption spectra for three molybdenum oxide species of known domain size.

erence series (top panel) decrease as the domain size increases. An analogous behavior is observed for the case of the Co:Mo (1:3)/ SiO_2 catalysts (bottom panel). An increase in the gap energy values is observed when the amount of Na in the catalysts increases. While for the undoped catalyst the energy gap lies between the values corresponding to $(\text{NH}_4)_6\text{Mo}_7\text{O}_{24}$ and MoO_3 , for the doped catalysts the energy gap shifts to higher values, indicating a decrease in the average size of the molybdenum domains. Indeed, for the catalyst with the higher loading of Na this value shifts up to 4.2 eV, which is very close to the value obtained for MoO_4^{2-} tetrahedral species. In agreement with the results obtained by Raman spectroscopy it is clear that the dispersion of oxidic molybdenum species is deeply influenced by the presence of sodium.

In addition to the charge-transfer bands due to Mo, appearing in the UV region, the visible spectra of these catalysts exhibit bands in the 500–750 nm region, which are associated with Co species and are ascribed to $d-d$ transitions ($^4\text{T}_{2g}$ to $^4\text{A}_{2g}$ and $^4\text{T}_{2g}$ to $^4\text{T}_{1g}$ (P)) of high spin octahedral Co complexes [38,39]. Fig. 3 shows the DRS spectra in this region for two Na-doped and an undoped Co:Mo (1:3)/ SiO_2 catalysts. The spectrum for the undoped catalyst is very similar to that of CoMoO_4 , in which Co is in an octahedral environment. The identical shape of the spectra of both samples indicates that the same type of ligand and symmetry around Co are common for the undoped catalyst and the cobalt molybdate. By contrast, the shape of the spectrum of the heavily doped catalyst is markedly different

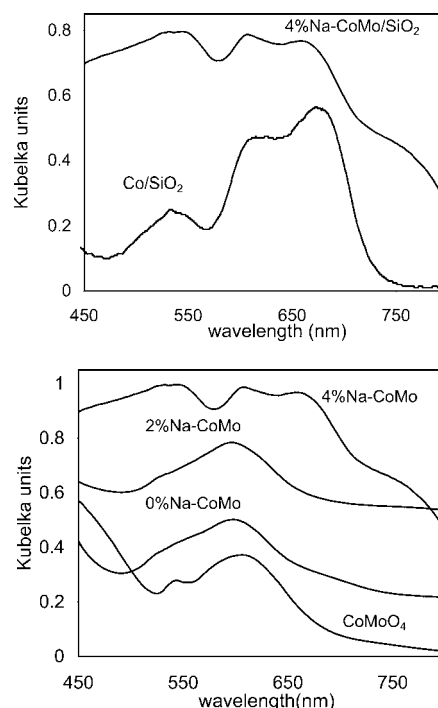


Fig. 3. Visible spectra obtained for an undoped and two Na-doped Co:Mo (1:3)/ SiO_2 catalysts compared to the spectra of a reference sample of cobalt molybdate (CoMoO_4). The spectrum obtained for a Co/ SiO_2 catalyst is also included for comparison.

and exhibits two new bands at around at 525 and 670 nm. These bands are in turn the characteristic features of the pure Co catalyst (Fig. 3 upper panel) and can be associated with Co_3O_4 species, which, as previously shown, are present in the fresh monometallic Co catalyst [8]. Therefore, it can be concluded that the addition of Na to the catalyst breaks up the interaction between Mo and Co in such a way that free Co oxide starts appearing. This conclusion is in perfect agreement with the Raman spectroscopy results.

3.1.3. Temperature-programmed reduction

The reduction profiles of the undoped and two Na-doped Co:Mo (1:3)/ SiO_2 catalysts in the precalcined state, together with those of the precalcined Co/ SiO_2 and Na-doped Mo/ SiO_2 , catalysts, are shown in Fig. 4a. The TPR profile of the precalcined Co catalyst shows two peaks at 360 and 445 °C, which can be ascribed to the reduction of Co oxide species. On the other hand, the reduction profile of the Na-doped Mo catalysts exhibits three different peaks that appear at much higher temperatures than those of Co. It is then pos-

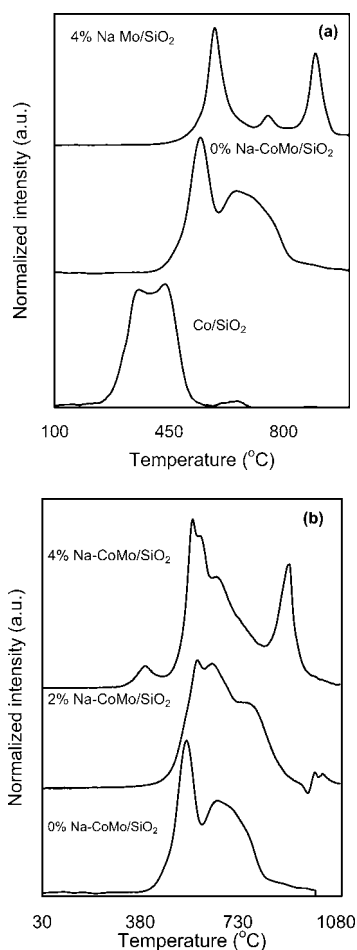


Fig. 4. (a) TPR profiles of a Co/ SiO_2 and Na-doped Mo/ SiO_2 catalysts compared to the undoped Co:Mo (1:3)/ SiO_2 bimetallic catalyst. (b) TPR profiles obtained for an undoped and two Na-doped Co:Mo (1:3)/ SiO_2 catalysts. In all cases the reduction was conducted under 5% H_2/Ar , using a heating linear ramp of 8 °C/min.

sible to use the reduction profiles to identify the presence of Co and Mo species in the absence of mutual interactions. Accordingly, the TPR of the undoped Co:Mo (1:3)/ SiO_2 catalyst indicates that, in this sample, the vast majority of Co oxide species are interacting with Mo. While most of the Co in the monometallic catalyst gets reduced below 500 °C, almost no reduction takes place below this temperature in the undoped bimetallic catalysts. It has been proposed that the addition of Mo oxide to Co oxide inhibits the reduction of the Co species because Mo^{6+} polarizes the Co–O bonds, making them more ionic and consequently more difficult to reduce [40]. In agreement with the Raman and UV–vis/DRS data, TPR indicates that a high degree of Co–Mo interaction is observed for the undoped Co:Mo (1:3)/ SiO_2 catalyst.

A contrasting behavior is observed in Fig. 4b. In this case, the TPR profiles of the Na-doped Co:Mo (1:3)/ SiO_2 catalyst are compared to the undoped catalyst. As shown in Fig. 4b, a gradually increasing fraction of segregated Co species as a function of the sodium content is apparent from the peak growing at 400 °C which is associated with the reduction of noninteracting Co oxide [41]. The observed trend agrees with the results obtained by UV–vis/DRS and Raman spectroscopy on the Na-doped catalysts. It is obvious that the fraction of cobalt interacting with Mo decreases with increasing Na content.

3.1.4. X-ray photoelectron spectroscopy (XPS)

XPS studies were performed on the air-calcined Na-doped and undoped catalysts to get an insight into the chemical state of the catalyst constituents. Fig. 5 shows the Co 2p spectra of the undoped and doped Co:Mo (1:3)/ SiO_2 catalysts compared to the spectra obtained for the monometallic Co/ SiO_2 , CoMoO_4 , and Co_3O_4 . As summarized in Table 1, the binding energies for the bimetallic catalysts seem to decrease as the Na content increases, which is the trend that one would expect if CoMoO_4 species in the catalyst are converted into Co_3O_4 species [40,42]. However, the values are too close to be conclusive. A more convincing evidence for this conversion is obtained by analyzing the shake-up satellite peaks appearing at 5–6 eV higher binding energies than the main peak in the Co 2p spectrum. The relative intensity of these satellite peaks has often been used for the identification of the cobalt species [43–45] since the intensities of the shake-up peaks satellites associated with the Co $2p_{3/2}$ of both oxides are quite different. As shown in Fig. 5, this satellite peak is very small in the spectrum of Co_3O_4 but very strong in the spectrum of cobalt molybdate, as previously observed [45,46]. Therefore, it is easy from the features of the Co 2p spectra to determine whether the Co species are present as cobalt molybdate or as cobalt oxide (Co_3O_4) on the catalyst. A clear trend is observed in Table 1 for the relative intensities. The intensity ratio for the undoped catalyst is high (0.6) and close to that of stoichiometric CoMoO_4 , but gradually approaches the value of cobalt oxide (0.3) as the Na content increases.

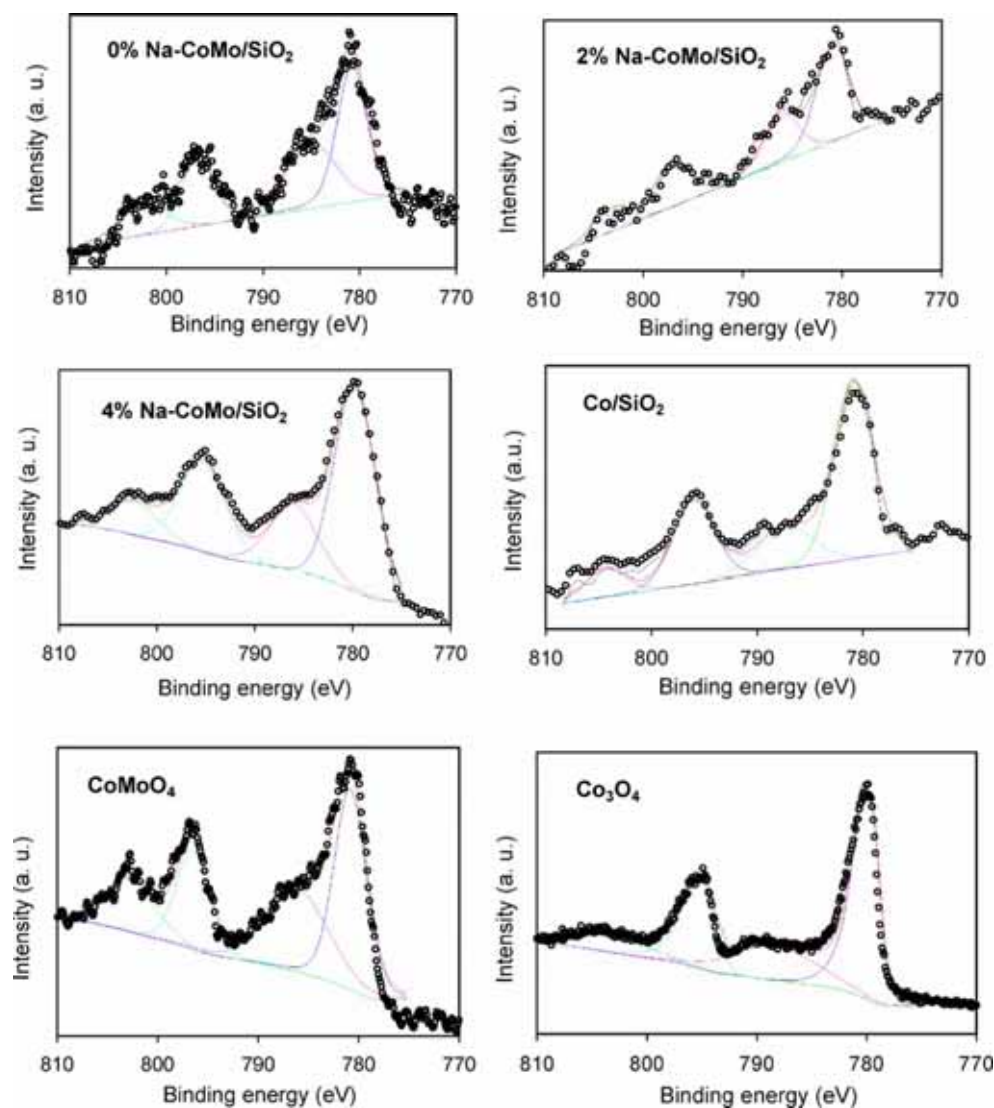


Fig. 5. XPS Co 2p spectra of an undoped and two Na-doped Co:Mo (1:3)/SiO₂ catalysts. The spectrum obtained for a monometallic Co/SiO₂ catalyst is also included for comparison. The spectra obtained for two reference samples of cobalt oxide Co₃O₄ and CoMoO₄ are also presented.

Table 1
Co 2p binding energies for undoped and Na-doped catalysts

| Catalyst | Co 2p _{3/2} peak position (eV) | Co 3p _{3/2} satellite peak position (eV) | Intensity ratio (Co 2p _{3/2} /satellite) |
|--|---|---|---|
| 0% Na–Co:Mo (1:3)/SiO ₂ | 780.9 | 785.5 | 0.60 |
| 2% Na–Co:Mo (1:3)/SiO ₂ | 780.6 | 786.5 | 0.58 |
| 4% Na–Co:Mo (1:3)/SiO ₂ | 779.5 | 786.5 | 0.33 |
| Co/SiO ₂ | 780.5 | 787.3 | 0.34 |
| Co ₃ O ₄ (reference) | 779.6 | 788.2 | 0.30 |
| CoMoO ₄ (reference) | 780.7 | 785.9 | 0.79 |

The position of the Co 2p_{1/2} satellite peak and its relative intensity is also indicated. The values obtained for two analytical samples of cobalt oxide Co₃O₄ and CoMoO₄ are also presented.

Fig. 6 shows the Mo 3d spectra of the doped and undoped Co:Mo (1:3)/SiO₂ catalysts. The values of the binding energies of the two spin orbit components ($3d_{5/2} = 232.0$ eV; $3d_{3/2} = 234.7$ eV) are characteristic of Mo(VI) species [47–49]. However an interesting difference can be

observed on the linewidth of the spectra. The linewidth of the Mo3d peaks obtained for the sample without sodium is wider than that for the Na-doped sample. This effect has been previously reported in the literature and has been attributed to the presence of monomeric MoO₄²⁻ species [45].

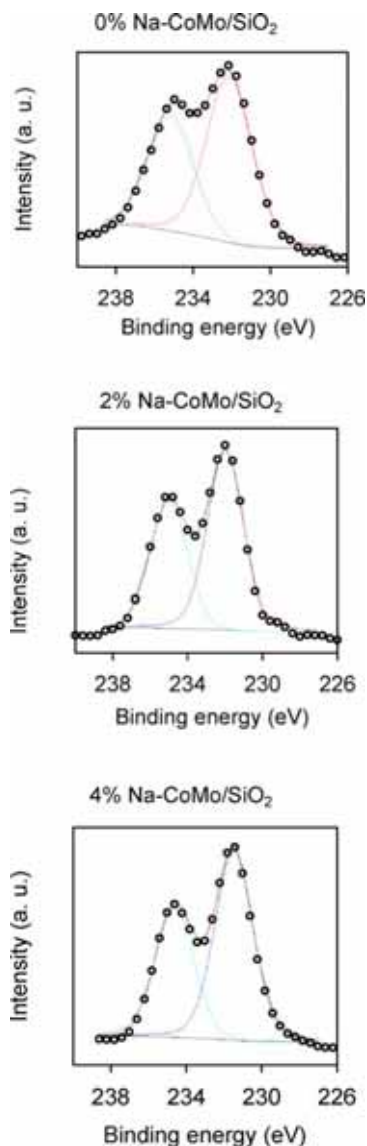


Fig. 6. XPS Mo 3d spectra of an undoped and two Na-doped Co:Mo (1:3)/SiO₂ catalysts. The spectra were fitted using Gaussian-Lorentzian functions to resolve the individual 3d_{5/2} and 3d_{3/2} contributions.

Even though this observation cannot be conclusive by itself, it perfectly agrees with the results obtained by Raman and UV-vis spectroscopy, which indicate that the dispersion of oxidic molybdenum species is deeply influenced by the presence of sodium.

3.2. Production and characterization of single-walled carbon nanotubes by catalytic disproportionation of CO

As we have reported in previous papers [6,8], the silica-supported Co-Mo system displays a very high selectivity in the production of single-wall nanotubes by CO disproportionation. Interestingly, the high yields and selectivities to SWNT were only obtained after a specific sequence of calcination at 500 °C in air and reduction in H₂ at 500 °C. In the present work, we compare the activity of undoped and Na-

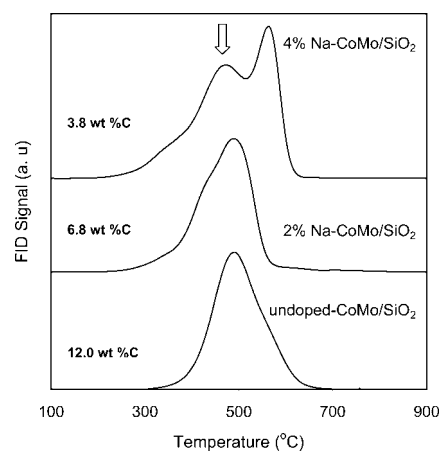


Fig. 7. Temperature-programmed oxidation profiles of all the carbonaceous species present in an undoped and two Na-doped Co:Mo (1:3)/SiO₂ catalysts after CO disproportionation at 850 °C for 2 h. The arrow indicates the center of the peak corresponding to the oxidation of SWNT. The total yield of carbon is also indicated.

doped Co:Mo (1:3)/SiO₂ catalysts for SWNT production. The reaction temperature employed for the CO disproportionation after a prereluction step was kept at 850 °C. At the end of a 2-h reaction period, the spent catalyst containing the carbon deposits was cooled down in He flow. The characterization of the carbon deposits was done by way of temperature-programmed oxidation, transmission electron microscopy, and Raman spectroscopy with varying excitation energy, three techniques that we have previously used and tested [6–8,52].

We have shown that from the TPO analysis one can obtain a quantitative measurement of the carbon yield and selectivity toward SWNT [6]. We have previously shown that under the TPO conditions and while still immersed on this particular catalyst, the SWNT are oxidized in a relatively narrow temperature range (maximum around 570 °C), which lies below the temperature in which MWNT, graphite, and carbon fibers are oxidized, but above the temperature at which amorphous and chemically impure carbon species are oxidized [7].

On the other hand, it is well known that a number of alkali metal oxides act as catalysts for the oxidation of carbon by gaseous oxidants [50]. These processes are generally thought to involve oxygen transfer steps in which the catalyst participates in a redox cycle between stoichiometric and substoichiometric oxide species [51]. As a consequence, one should expect that the presence of sodium can affect the oxidation process. Fig. 7 shows the TPO profile of the undoped CoMo catalyst in which sodium was added after SWNT synthesis in order to account for the presence of the alkali metal in the TPO. The postaddition of Na only results in a shift from 570 °C as observed without Na [6] to 450 °C. This shift clearly demonstrates the catalytic influence of Na in the oxidation process. However, it is important to point out that the shape or number of peaks has not been affected. Therefore, it is still possible to obtain information about the

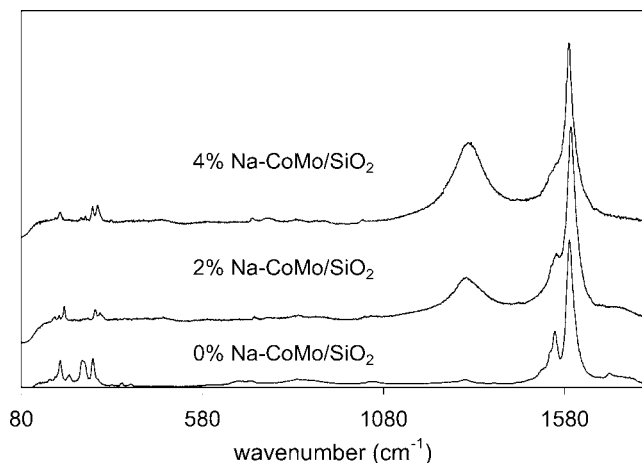


Fig. 8. (a) Raman spectra of the carbon deposits obtained by disproportionation of CO at 850 °C over an undoped and two Na-doped Co:Mo (1:3)/SiO₂ catalysts after a pretreatment at 500 °C in hydrogen. The laser excitation energy was 633 nm.

different kinds of carbon species from the TPO profiles. For instance, Fig. 7 illustrates the strong influence of the presence of sodium in yield and selectivity during the SWNT growth. As noted above, the TPO profile of the product obtained over the undoped Co:Mo (1:3)/SiO₂ catalyst displays a single TPO peak centered at 450 °C. A contrasting behavior is observed in the TPO profile of the material obtained over the 4% Na-doped catalysts (see Fig. 7). Instead of the single TPO peak observed in the previous case, three oxidation peaks are obtained on this sample. Although it is not possible to make a direct assignment of the different carbon species that originate each of the different peaks in the TPO profile based solely on the TPO data [52], this result clearly indicates a decrease in the selectivity to SWNT originated by the presence of sodium in the catalyst.

Raman spectroscopy is another useful technique for evaluating the structure of carbon nanotubes. As noted above, from the position of the radial breathing mode band, direct information about the tubes diameter can be obtained [21] while the relative intensity of the D band relative to the G band is widely used as qualitative measurement of the formation of undesirable forms of carbon [22,23]. Fig. 8 shows typical Raman spectra obtained on the carbon deposits formed on the undoped and doped Co:Mo (1:3)/SiO₂ catalysts. Depending on the amount of sodium present on the catalysts a pronounced variation is observed in the relative intensity of the D band. As a matter of fact Fig. 8 shows that the SWNT material obtained over the undoped catalyst is of high quality, while the samples obtained in both Na-doped catalysts show much lower quality, which undoubtedly indicates the presence of undesirable forms of carbon. In agreement with the results obtained by TPO analysis, it is evident that the presence of Na has a negative impact on the selectivity of the Co:Mo (1:3)/SiO₂ catalysts.

The TEM observations fully support the results of the other techniques. As shown in Fig. 9, a contrasting differ-

ence is observed on the carbon structures produced with an undoped CoMo catalyst and with a heavily Na-doped sample. While the sample obtained over the undoped catalyst exhibited a high density of SWNT, the sample obtained with the 4% Na-doped catalyst mainly produced defective MWNT and graphitic carbon deposits. In the first case, one can observe the typical parallel lattice fringes characteristic of SWNT, while in the second case, a spacing of 0.34 nm can be observed between the fringes, which is the characteristic value for the lattice space between individual walls of graphitic fibers [53].

4. Discussion

In previous reports we have discussed the characterization results obtained on the undoped Co:Mo system used for SWNT production [8]. The most important conclusions of such studies were that the extent of the Co–Mo interaction strongly depended on the Co:Mo molar ratio in the catalyst and that this interaction had diverse forms during the various stages of the catalyst life. For instance, we were able to establish that in the calcined state, Mo was in the form of a well-dispersed Mo(VI) oxide while the state of Co strongly depended on the Co:Mo ratio. At low Co:Mo ratios, it interacted with Mo forming a superficial Co molybdate-like structure. At high Co:Mo ratios, it forms a noninteracting Co₃O₄ phase. During the subsequent reduction treatment in hydrogen, the noninteracting Co phase reduced to metallic Co, while the Co molybdate-like species remained as well-dispersed Co²⁺ ions.

We demonstrated that the effect of having Co stabilized in the Co-molybdate environment was critical for a good performance during the nanotube growth. First of all, this stabilization avoided the sintering of Co into large metallic aggregates, which generate undesired forms of carbon, as it occurs when the noninteracting cobalt oxide phase gets reduced before nanotube growth. By contrast, in the selective catalyst, Co clusters are only formed after the Mo oxide has become Mo carbide, thus breaking the Co–Mo interaction. Under the reaction conditions (high temperature and CO pressure), CO dissociates on the nascent Co clusters and carbon atoms begin to nucleate over Co and generate the nanotube cap that is the precursor of the single-walled nanotube.

The characterization results for the Na-doped Co–Mo catalyst series reported in this work can be put together in an analogous picture. For instance the Raman, UV–vis/DRS, and XPS data clearly indicate that the dispersion of molybdenum has been strongly affected by the presence of sodium in the catalyst. Furthermore, the development of new bands in the Raman spectra as well as the values of the gap energies (Fig. 2) clearly indicates that molybdenum is interacting with the Na dopant forming sodium molybdate moieties in the catalyst. In fact, it has been argued that alkali ion impurities such Na⁺ or K⁺ have higher affinity for molybdenum

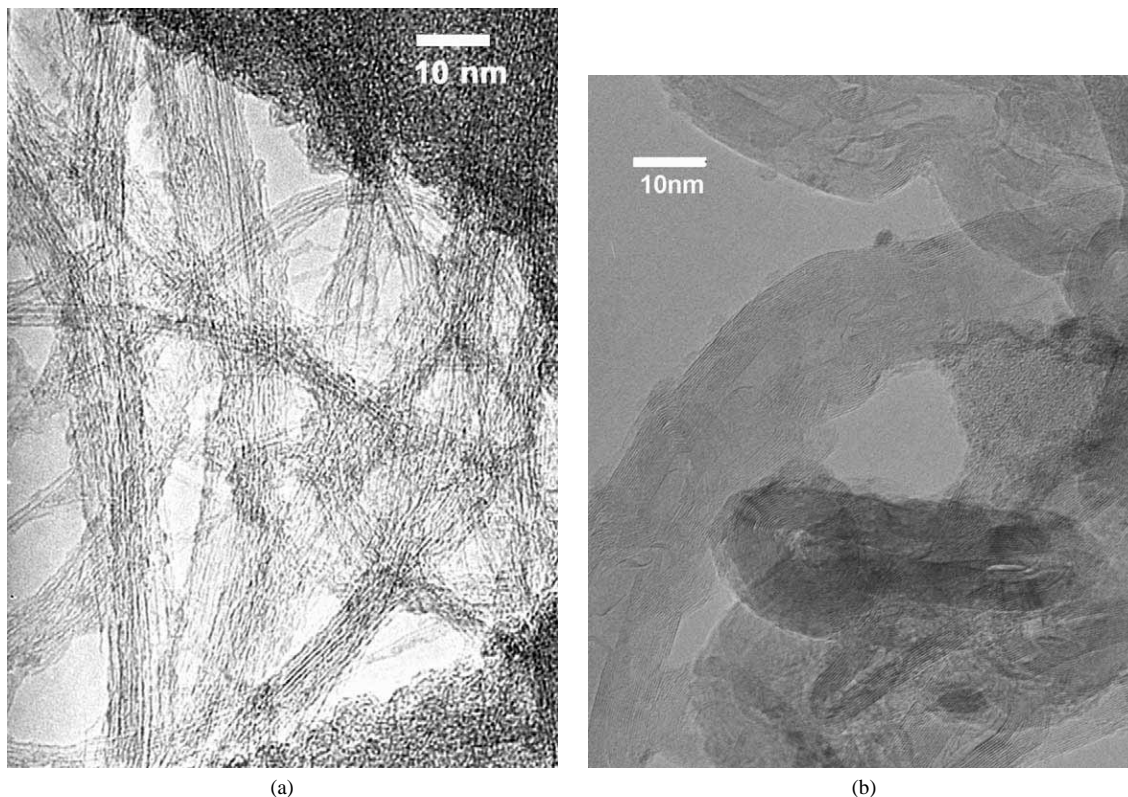


Fig. 9. (a) TEM images showing SWNT produced by CO disproportionation over an undoped Co:Mo (1:3)/SiO₂ catalyst. (b) TEM images showing a mixture of MWNT and graphite produced by CO disproportionation over a 4% Na-doped Co:Mo (1:3)/SiO₂ catalyst.

species than the silica support [19,54], although still some disagreement remains on this particular topic [17]. Another plausible explanation could be that the presence of alkaline ions results in an increase of the surface pH values at the point of zero charge (PZC). Thus when Na is present, large molybdenum oxide polyanions become less favorable to monomeric species [55]. In either case, it is clear that the presence of sodium deeply changes the dispersion of molybdenum species.

When these sodium molybdate monomeric species are formed, the interaction of molybdenum and cobalt is hindered. In fact the Raman, UV-vis/DRS, TPR, and XPS results clearly show that a segregated phase of cobalt oxide (Co₃O₄) is formed. In this context, it is important to note that a Na excess is needed to break the Co–Mo interaction in the cobalt molybdate phase. For example, the UV-vis/DRS data clearly show that a relative large amount of sodium (i.e., 4 wt%) must be added to the catalyst before a noninteracting Co oxide phase begins to form. The Raman spectra (Fig. 1b) together with the results obtained from X-ray photoelectron spectroscopy (Fig. 5) undoubtedly show that this noninteracting phase is Co₃O₄. These results are schematically represented in Fig. 10.

In previous reports [8], we have proposed that the role of Co is the activation of CO, while the role of Mo is the stabilization of Co(II) ions. When Co is not interacting with Mo, in the reduced state it sinters and forms large metal aggregates. These large metallic Co aggregates have the ten-

dency to generate defective MWNT, carbon filaments, and graphite nanofibers. As noted above, when Mo is present in the catalyst and there is no excess of free Co, a well-dispersed Co⁺² species in the form of a Co molybdate-like phase is stabilized. From the detailed studies conducted over the Na-doped Co–Mo system reported in this contribution, we can propose that the disruption by sodium of the cobalt–molybdenum interaction is responsible for the loss of selectivity toward the formation of SWNT in the catalyst. The driving force for this disruption is either the tendency of Na to form sodium molybdate or the change of the surface pH values. The disruption of the Co–Mo interaction causes the segregation of cobalt into a new Co₃O₄ phase. As a consequence, the Na-doped catalyst shows a low selectivity because the ability of a Co–Mo catalyst to form SWNT depends on the formation of the surface cobalt molybdate species.

5. Conclusions

We can summarize the main findings of the present work in the following conclusions:

1. The presence of sodium deeply affects the dispersion of molybdenum. In the undoped catalyst, molybdenum forms small aggregates with domain size close to that of

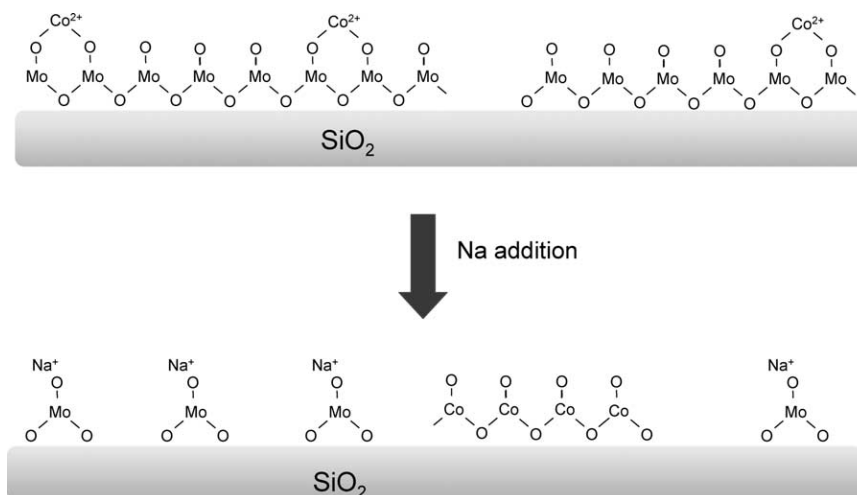


Fig. 10. Schematic description of the structure of the Co:Mo (1:3)/SiO₂ catalyst with and without sodium as derived from the characterization methods.

heptamolybdate species while in the case the doped catalyst monomeric sodium molybdate species are formed.

2. When sodium molybdate species are formed, the interaction between molybdenum and cobalt is disrupted and a new phase of segregated Co₃O₄ is formed.
3. During the reduction pretreatment, the noninteracting Co₃O₄ phase is reduced to metallic Co, which easily sinters at the nanotube growth conditions. Large Co particles generate defective MWNT, carbon filaments, and graphite nanofibers under reaction conditions, originating a loss in selectivity of the Co–Mo catalyst.

Acknowledgments

This research was conducted with financial support from the Department of Energy, Office of Basic Energy Sciences (Grant DE-FG03-02ER15345). One of us (J.E.H.) thanks the Fulbright-CAREC program for a scholarship. We acknowledge Walter E. Alvarez and Leandro Balzano for helpful discussions.

References

- [1] B.I. Yakobson, R.E. Smalley, *Am. Scientist* 85 (1997) 324.
- [2] Y. Saito, T. Nakahira, S. Uemura, *J. Phys. Chem. B* 107 (2003) 931.
- [3] B.Q. Wei, R. Vajtai, P.M. Ajayan, *Carbon* 41 (2003) 185.
- [4] J. Gavillet, A. Loiseau, F. Ducastelle, S. Thair, P. Bernier, O. Stephan, J. Thibault, J.-C. Charlier, *Carbon* 40 (2002) 1649.
- [5] J.-C. Charlier, S. Iijima, *Top. Appl. Phys.* 80 (2001) 55.
- [6] B. Kitiyanan, W.E. Alvarez, J.H. Harwell, D.E. Resasco, *Chem. Phys. Lett.* 317 (2000) 497.
- [7] W.E. Alvarez, B. Kitiyanan, A. Borgna, D.E. Resasco, *Carbon* 39 (2001) 547.
- [8] J.E. Herrera, L. Balzano, A. Borgna, W.E. Alvarez, D.E. Resasco, *J. Catal.* 204 (2001) 129.
- [9] J.V. Lauritsen, S. Helveg, E. Lægsgaard, I. Stensgaard, B.S. Clausen, H. Topsøe, F. Besenbacher, *J. Catal.* 197 (2001) 1.
- [10] H. Topsøe, B.S. Clausen, *Catal. Rev. Sci. Eng.* 26 (1984) 395.
- [11] S.M.A.M. Bouwens, R. Prins, V.H.J. de Beer, D.C. Koningsberger, *J. Phys. Chem.* 94 (1990) 3711.
- [12] S.M.A.M. Bouwens, J.A.R. van Veen, D.C. Koningsberger, V.H.J. de Beer, R. Prins, *J. Phys. Chem.* 95 (1991) 123.
- [13] A.M. Venezia, V. La Parola, A. Longo, A. Martorana, *J. Solid State Chem.* 161 (2001) 373.
- [14] A.M. Venezia, F. Raimondi, V. La Parola, G. Deganello, *J. Catal.* 194 (2000) 393.
- [15] G. Muralidhar, F.E. Massoth, J. Shabtai, *J. Catal.* 85 (1984) 44.
- [16] G. Xiong, Z. Feng, J. Li, Q. Yang, P. Ying, Q. Xin, C. Li, *J. Phys. Chem. B* 104 (2000) 3581.
- [17] G. Mestl, T.K.K. Srinivasan, *Catal. Rev.-Sci. Eng.* 40 (1998) 451.
- [18] N.F.D. Verbruggen, L.M.J. von Hippel, G. Mestl, B. Lengeler, H. Knoezinger, *Langmuir* 10 (1994) 3073.
- [19] M.A. Bañares, N.D. Spencer, M.D. Jones, I.E. Wachs, *J. Catal.* 146 (1994) 204.
- [20] C.C. Williams, J.G. Ekerdt, J.M. Jehng, F.D. Hardcastle, A.M. Turek, I.E. Wachs, *J. Phys. Chem.* 95 (1991) 8781.
- [21] A.M. Rao, E. Richter, S. Bandow, B. Chase, P.C. Eklund, K.A. Williams, S. Fang, K. Subbaswamy, M. Menon, A. Thess, R.E. Smalley, G. Dresselhaus, M.S. Dresselhaus, *Science* 275 (1997) 187.
- [22] S. Rols, A. Righi, L. Alvarez, E. Anglaret, R. Almairac, C. Journet, P. Bernier, J.L. Sauvajol, A.M. Benito, W.K. Maser, E. Munoz, M.T. Martinez, G.F. de la Fuente, A. Girard, J.C. Ameline, *Eur. Phys. J. B* 18 (2000) 201.
- [23] S. Bandow, S. Asaka, Y. Saito, A.M. Rao, L. Grigorian, E. Richter, P.C. Eklund, *Phys. Rev. Lett.* 80 (1998) 3779.
- [24] M.A. Vuurman, I.E. Wachs, *J. Mol. Catal.* 77 (1992) 29.
- [25] A.R. Saini, B.G. Johnson, F.E. Massoth, *Appl. Catal.* 40 (1988) 157.
- [26] B. Vielhaber, H. Knözinger, *Appl. Catal.* 26 (1986) 375.
- [27] F.R. Brown, L.E. Makovsky, K.H. Rhee, *J. Catal.* 50 (1977) 162.
- [28] V. La Parola, G. Deganello, C.R. Tewell, A.M. Venezia, *Appl. Catal. A* 235 (2002) 171.
- [29] R. Radhakrishnan, C. Reed, S.T. Oyama, M. Seman, J.N. Kondo, K. Domen, Y. Ohminami, K. Asakura, *J. Phys. Chem. B* 105 (2001) 8519.
- [30] Z. Li, Y. Fu, J. Bao, M. Jiang, T. Hu, T. Liu, Y.-N. Xie, *Appl. Catal. A* 220 (2001) 21.
- [31] G.M. Clark, W.P. Doyle, *Spectrochim. Acta* 22 (1966) 1441.
- [32] F. Trifiro, P. Centola, I. Pasquon, *J. Catal.* 10 (1968) 86.
- [33] W. Kuang, Y. Fan, K. Chen, Y. Chen, *J. Catal.* 186 (1999) 310.
- [34] K. Nakamoto, *Infrared and Raman Spectra of Inorganic and Coordination Compounds*, third ed., Wiley, New York, 1986.
- [35] V.G. Hadjiev, M.N. Iliev, I.V. Vergilov, *J. Phys. C* 21 (1988) L199.
- [36] D.G. Barnton, M. Shtein, R.D. Wilson, S.L. Soled, E. Iglesia, *J. Phys. Chem. B* 103 (1999) 630.

- [37] R.S. Weber, *J. Catal.* 151 (1995) 470.
- [38] H. Kasper, *Monatsh. Chem.* 98 (1967) 2104.
- [39] P. Gajardo, P. Grange, B. Delmon, *J. Phys. Chem.* 83 (1979) 1771.
- [40] S. Halawy, M. Mohamed, G. Bond, *J. Chem. Tech. Biotechnol.* 58 (1993) 237.
- [41] J. Li, G. Jacobs, Y. Zhang, T. Das, B.H. Davis, *Appl. Catal. A* 223 (2002) 195.
- [42] R. Kleyna, H. Mex, M. Voß, D. Borgmann, L. Viscido, J.M. Heras, *Surf. Sci.* 433 (1999) 723.
- [43] R.L. Chin, D.M. Hercules, *J. Phys. Chem.* 86 (1982) 3079.
- [44] F.B. Noronha, C.A. Perez, R. Frety, M. Schmal, *Phys. Chem. Chem. Phys.* 1 (1999) 2861.
- [45] A.M. Venezia, V. La Parola, G. Deganello, D. Cauzzi, C. Leonardi, G. Predieri, *Appl. Catal. A* 229 (2002) 261.
- [46] Y. Okamoto, T. Imanaka, S. Teranishi, *J. Catal.* 65 (1980) 448.
- [47] F. Solymosi, J. Cserényi, A. Szöke, T. Bánsági, A. Oszkó, *J. Catal.* 165 (1997) 150.
- [48] A. Katrib, P. Leflaive, L. Hilaire, G. Maire, *Catal. Lett.* 38 (1996) 95.
- [49] L. Coulier, V.H.J. de Beer, J.A. R van Veen, J.W. Niemantsverdriet, *Top. Catal.* 13 (2000) 99.
- [50] D.W. McKee, *Carbon* 25 (1987) 587.
- [51] H.Y. Huang, R.T. Yang, *J. Catal.* 185 (1999) 286.
- [52] J.E. Herrera, D.E. Resasco, *Chem. Phys. Lett.* 376 (2003) 302.
- [53] T.W. Ebbesen, P.M. Ajayan, *Nature* 358 (1992) 220.
- [54] M.A. Bañares, H. Hu, I.E. Wachs, *J. Catal.* 150 (1994) 407.
- [55] R.J. Hunter, in: R.H. Ottewill, R.L. Rowell (Eds.), *Zeta Potential in Colloid Science, Principle and Application in Colloid Science*, Academic Press, London, 1988, p. 233.